Supplementary material : Phosphate Boosting Stable Efficient Seawater Splitting on Porous NiFe (oxy)hydroxide@$NiMoO_4$ Core-Shell Micropillar Electrode

Chen Yang[#,1,2], Nannan Gao[#,1,3], Xilong Wang[1], Jiajia Lu[1], Lijuan Cao[1,3], Yadong Li[1,2], Han-Pu Liang[1,2,4]

[1]Qingdao Institute of Bioenergy and Bioprocess Technology, Chinese Academy of Sciences, Qingdao, 266101, China

[2]Center of Materials Science and Optoelectronics Engineering, University of Chinese Academy of Sciences, Beijing, 100049, China

[3]Sino-danish college, University of Chinese Academy of Sciences, Beijing, 101408, China

[4]Dalian National Laboratory for Clean Energy, Dalian, 116023, China

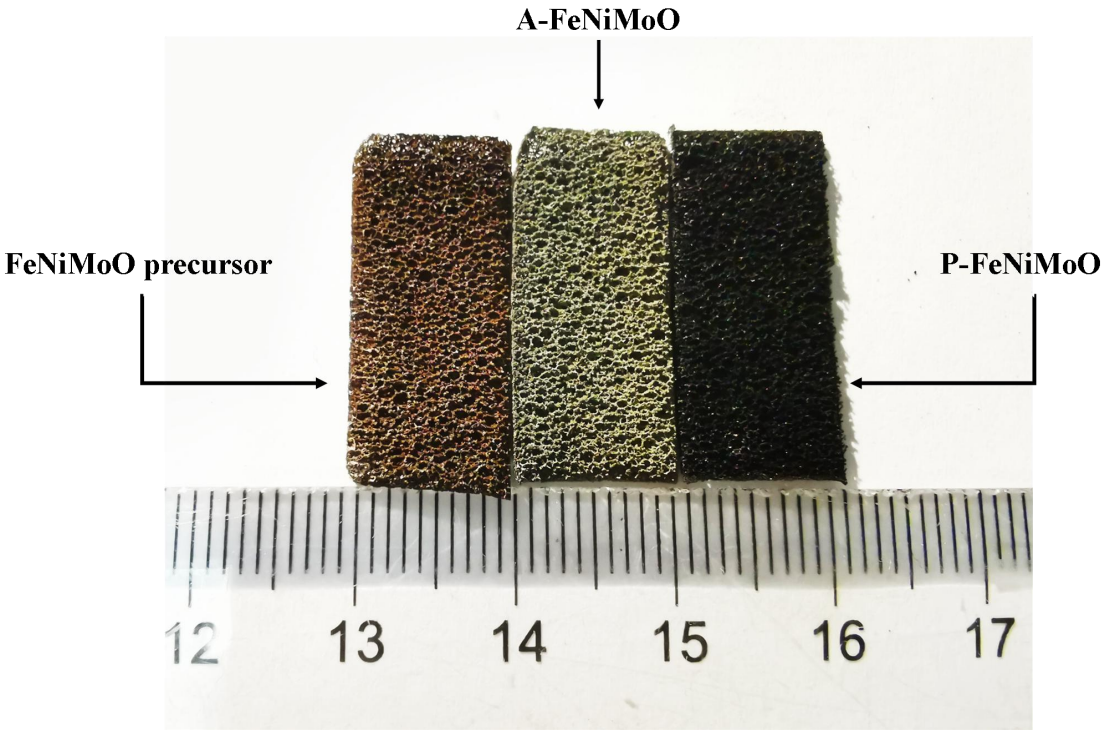

Supplementary Figure 1. Optical image of FeNiMoO precursor (L), A-FeNiMoO (M), and P-FeNiMoO (R) on nickel foam.

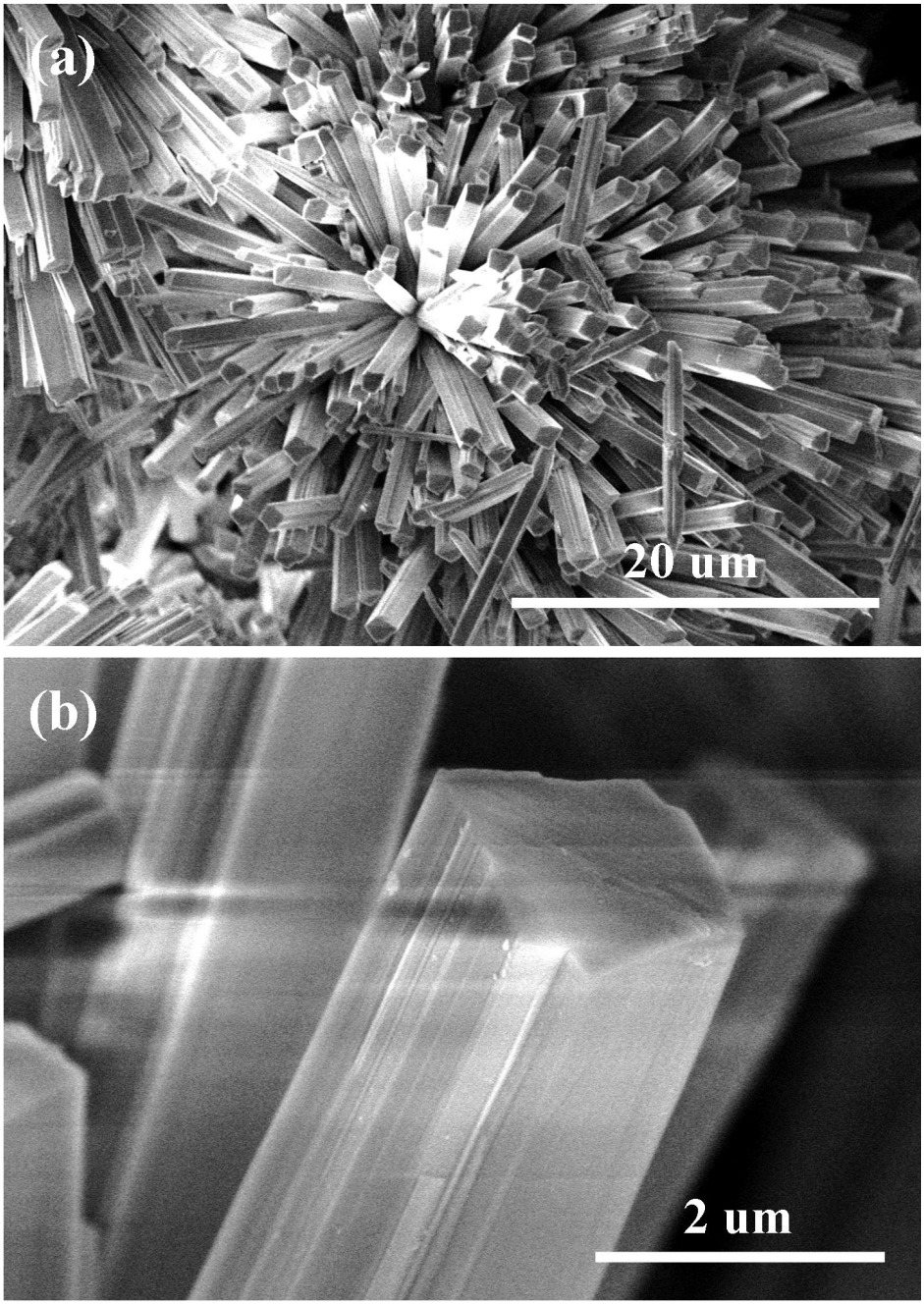

Supplementary Figure 2. (a) Low and (b) high magnification SEM images of FeNiMoO precursor electrode.

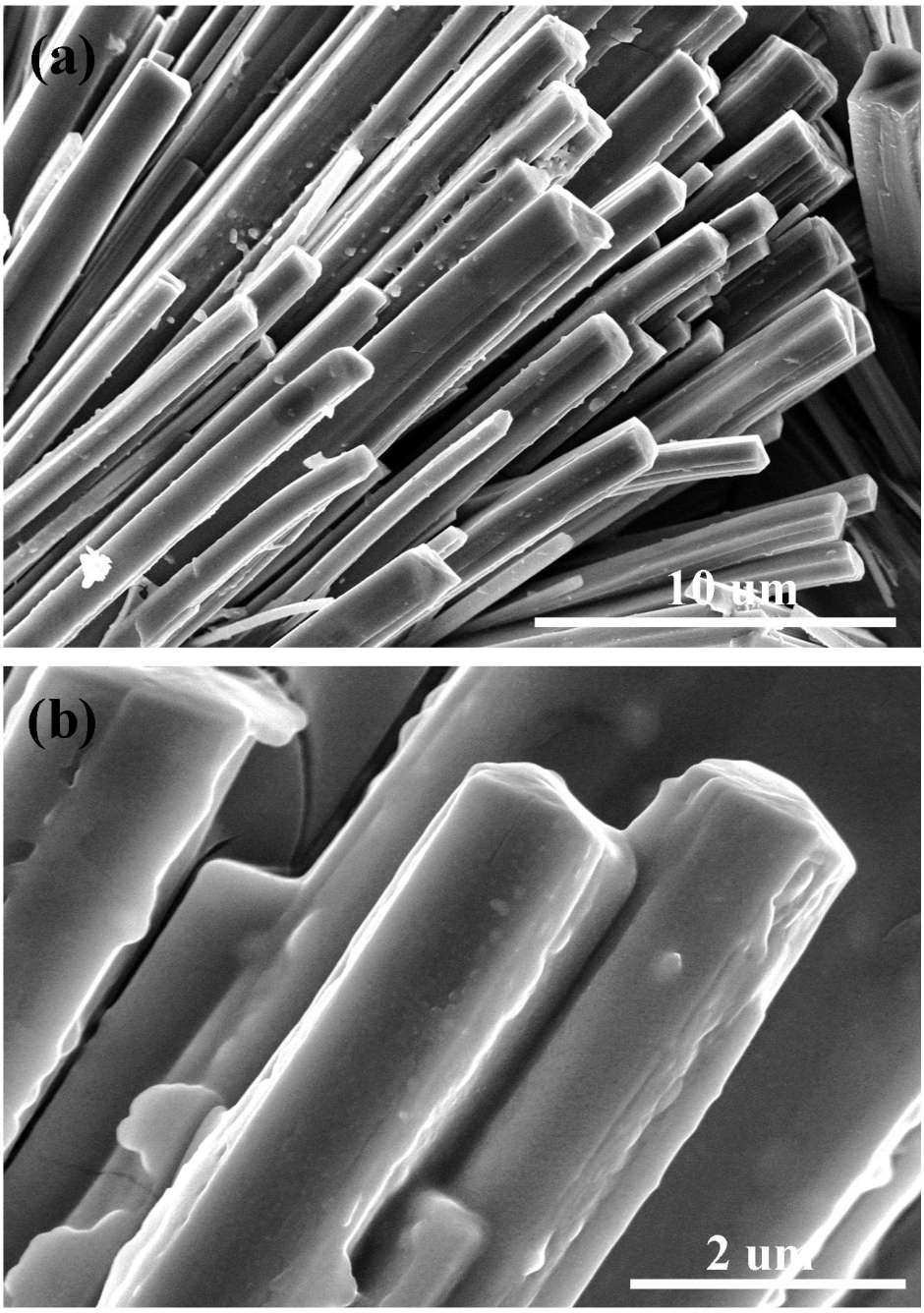

Supplementary Figure 3. (a) Low and (b) high magnification SEM images of P-FeNiMoO electrode.

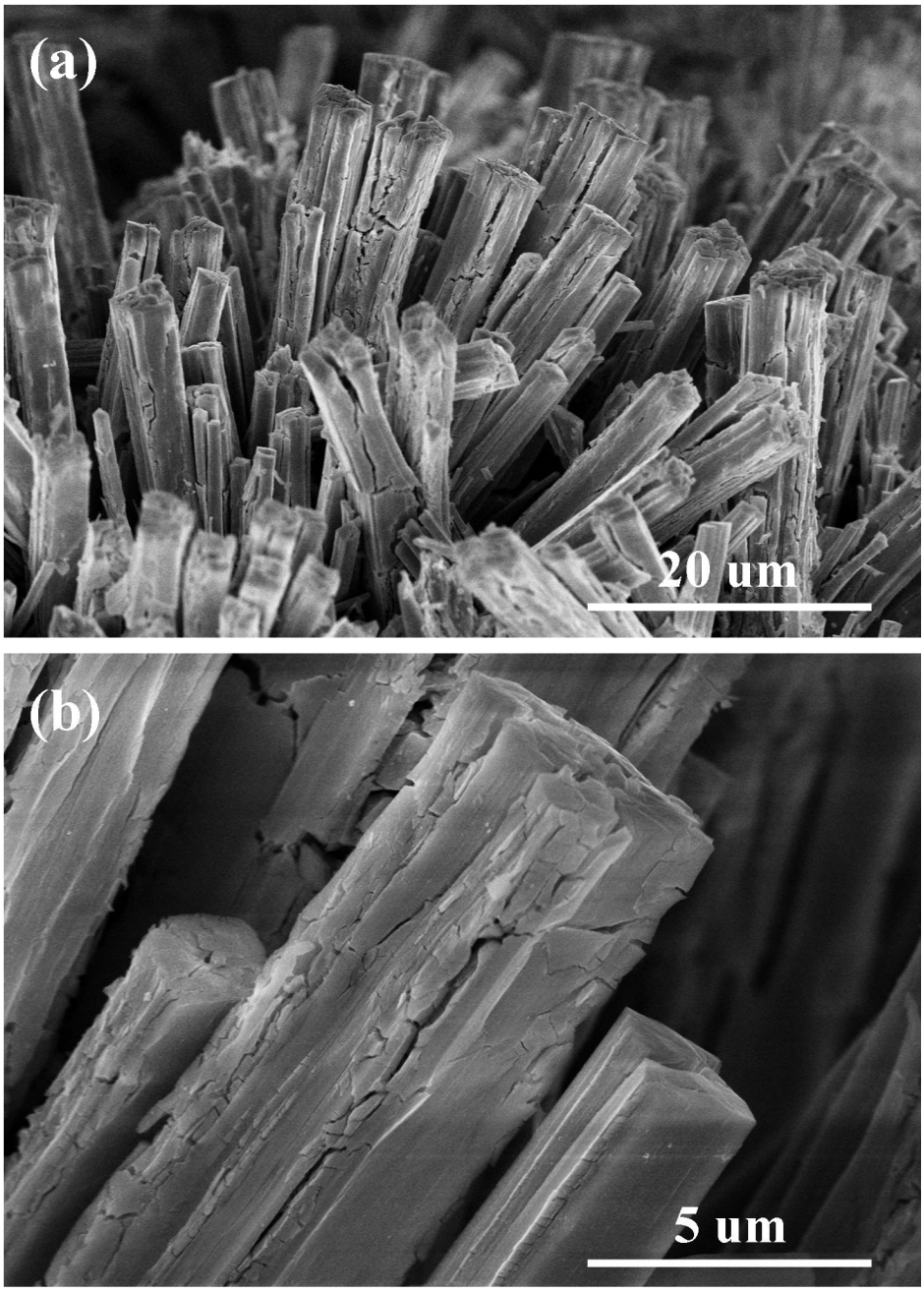

Supplementary Figure 4. SEM images of A-FeNiMoO on nickel foam at (a) low and (b) high magnification.

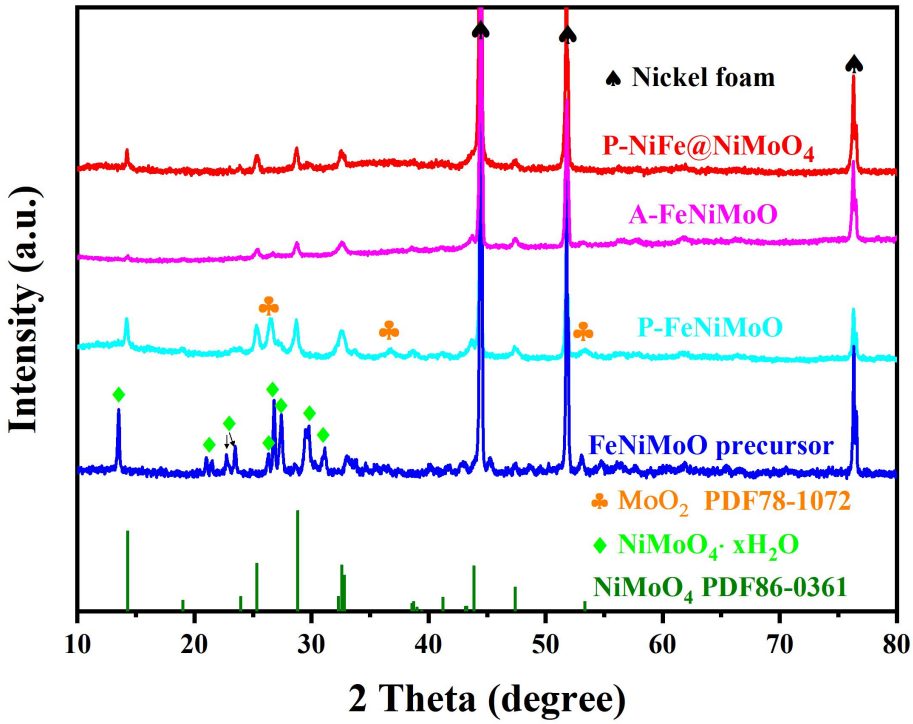

Supplementary Figure 5. XRD patterns for FeNiMoO precursor, A-FeNiMoO, P-FeNiMoO, and P-NiFe@$NiMoO_4$.

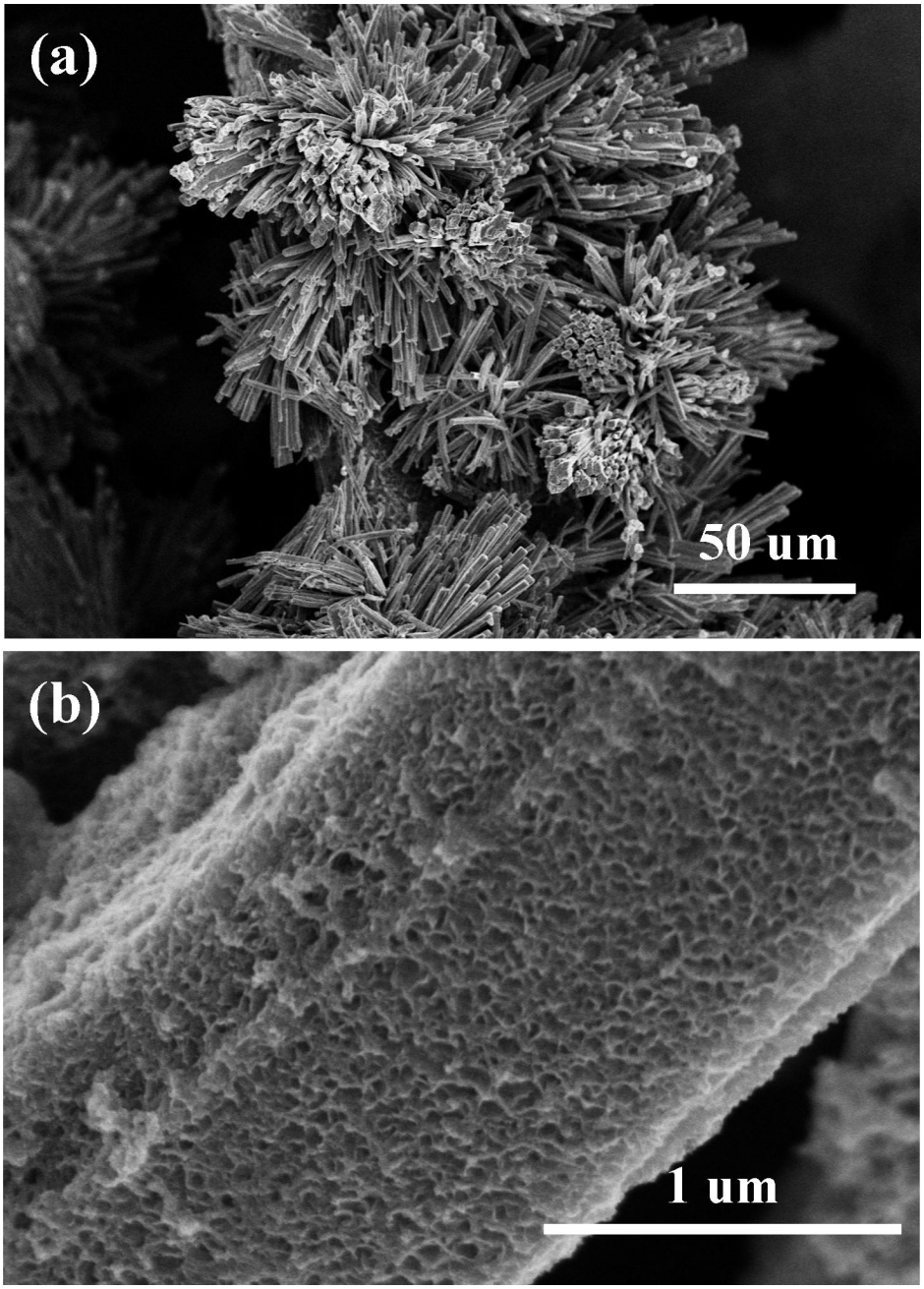

Supplementary Figure 6. SEM images of P-NiFe@$NiMoO_4$ on nickel foam.

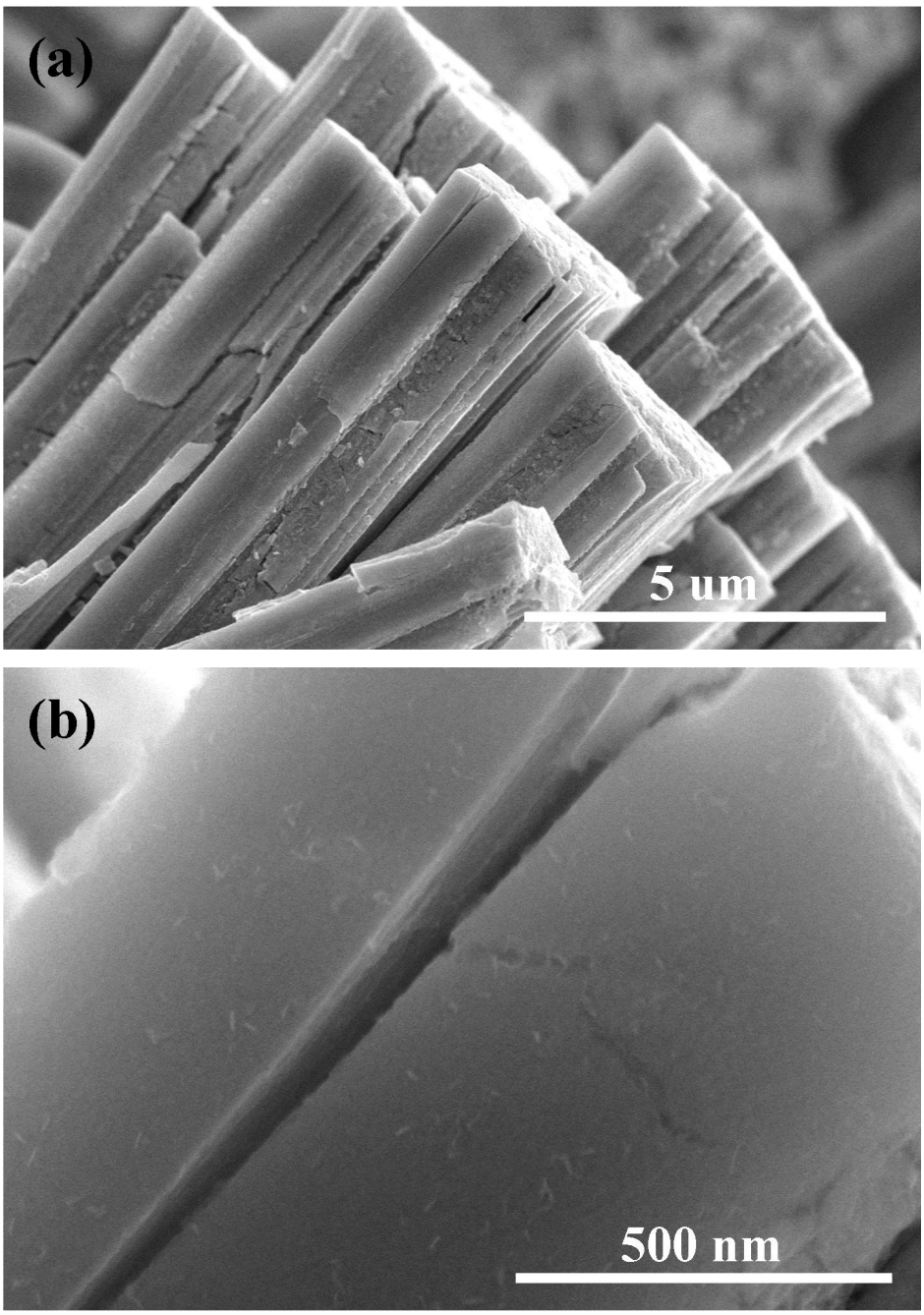

Supplementary Figure 7. SEM images of A-NiFe@$NiMoO_4$ electrode at (a) low and (b) high magnification.

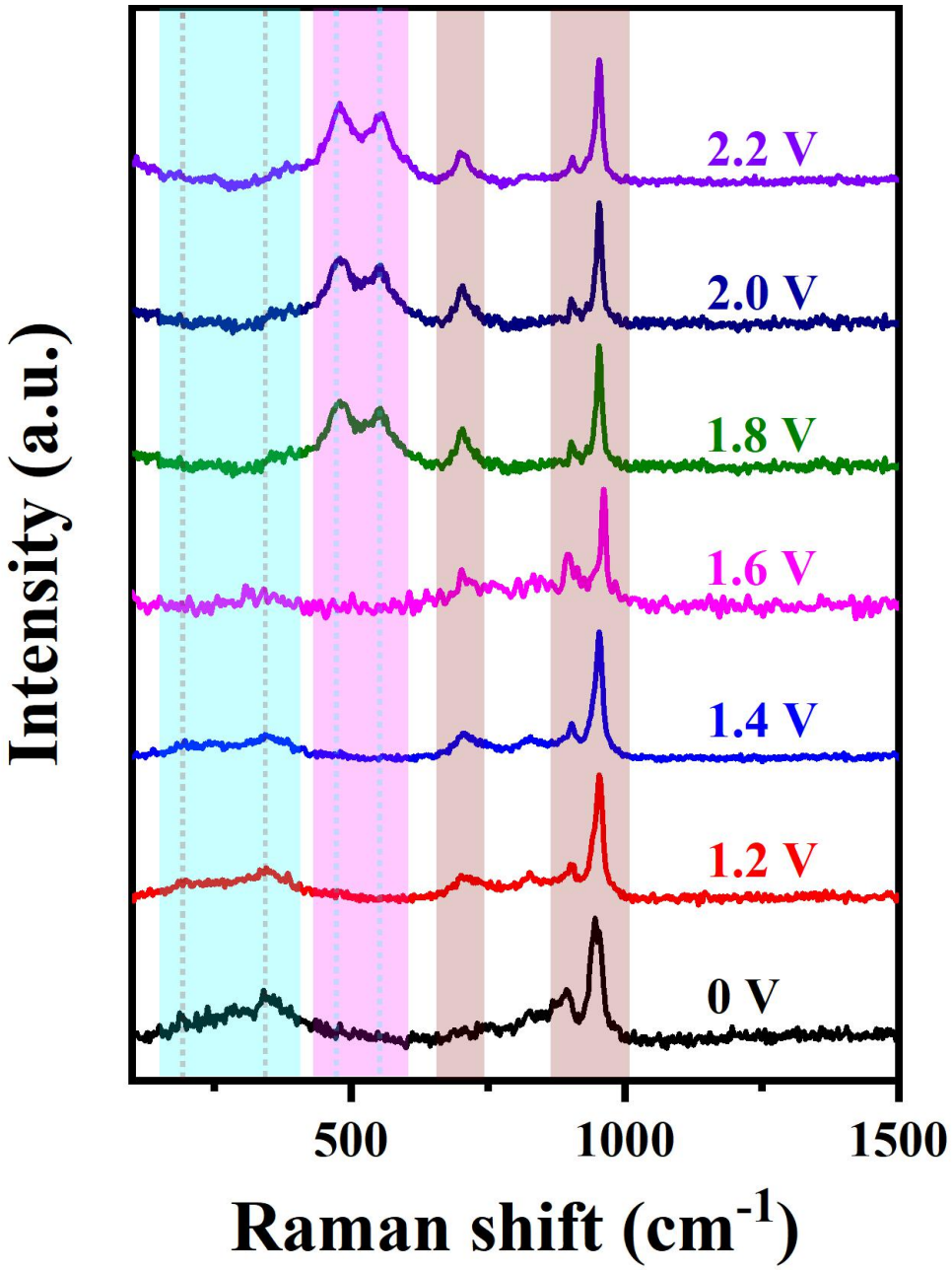

Supplementary Figure 8. In-situ Raman spectra of P-NiFe@NiMoO4 measured at various potentials versus RHE in 1 M KOH.

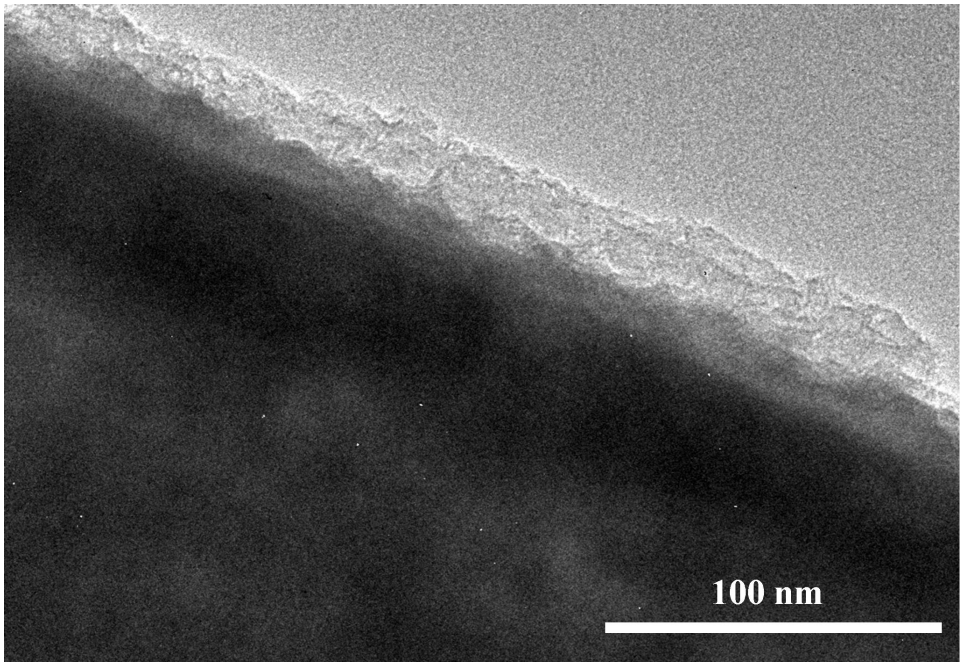

Supplementary Figure 9. TEM images of P-NiFe@$NiMoO_4$ electrode.

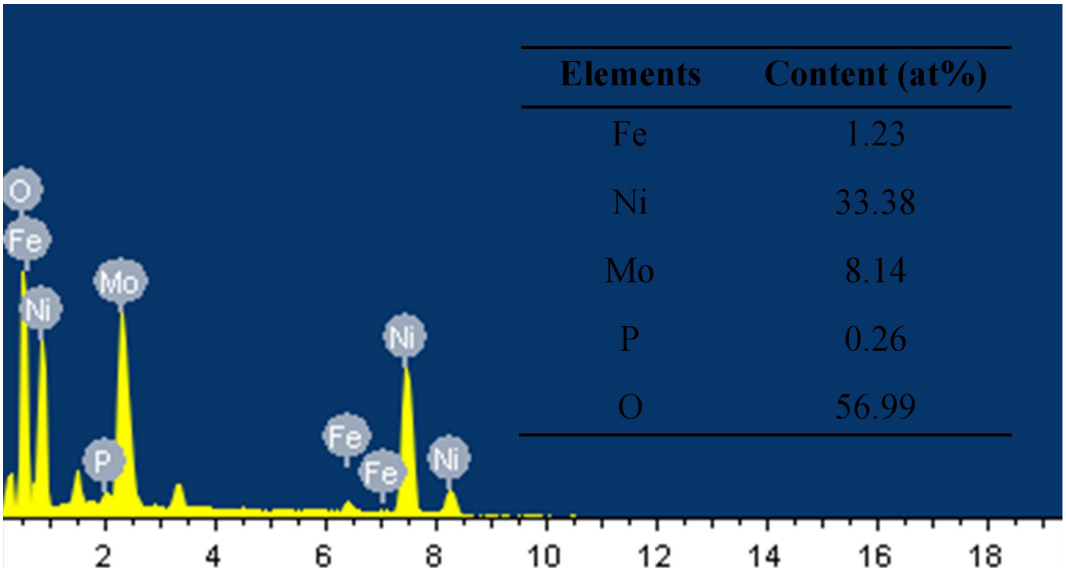

Elements	Content (at%)
Fe	1.23
Ni	33.38
Mo	8.14
P	0.26
O	56.99

Supplementary Figure 10. EDS elemental composition analysis of P-NiFe@$NiMoO_4$.

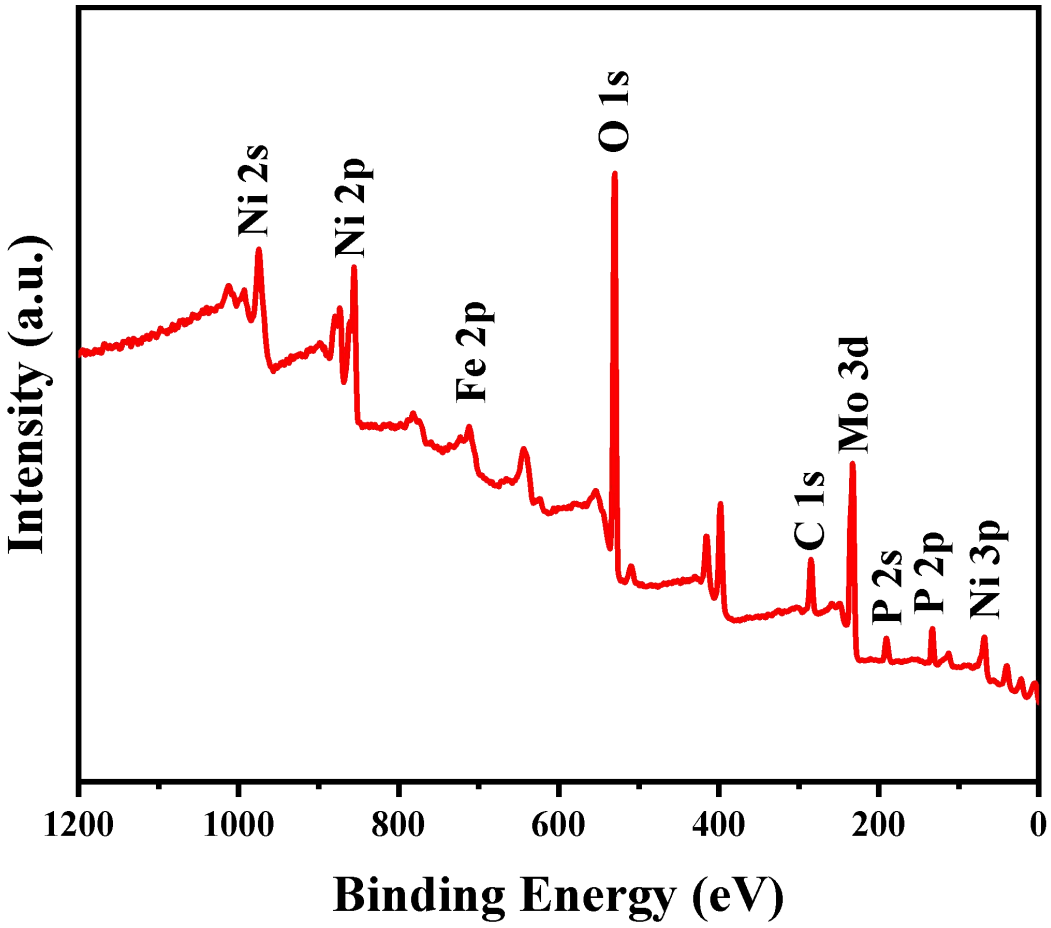

Supplementary Figure 11. XPS survey of P-FeNiMoO.

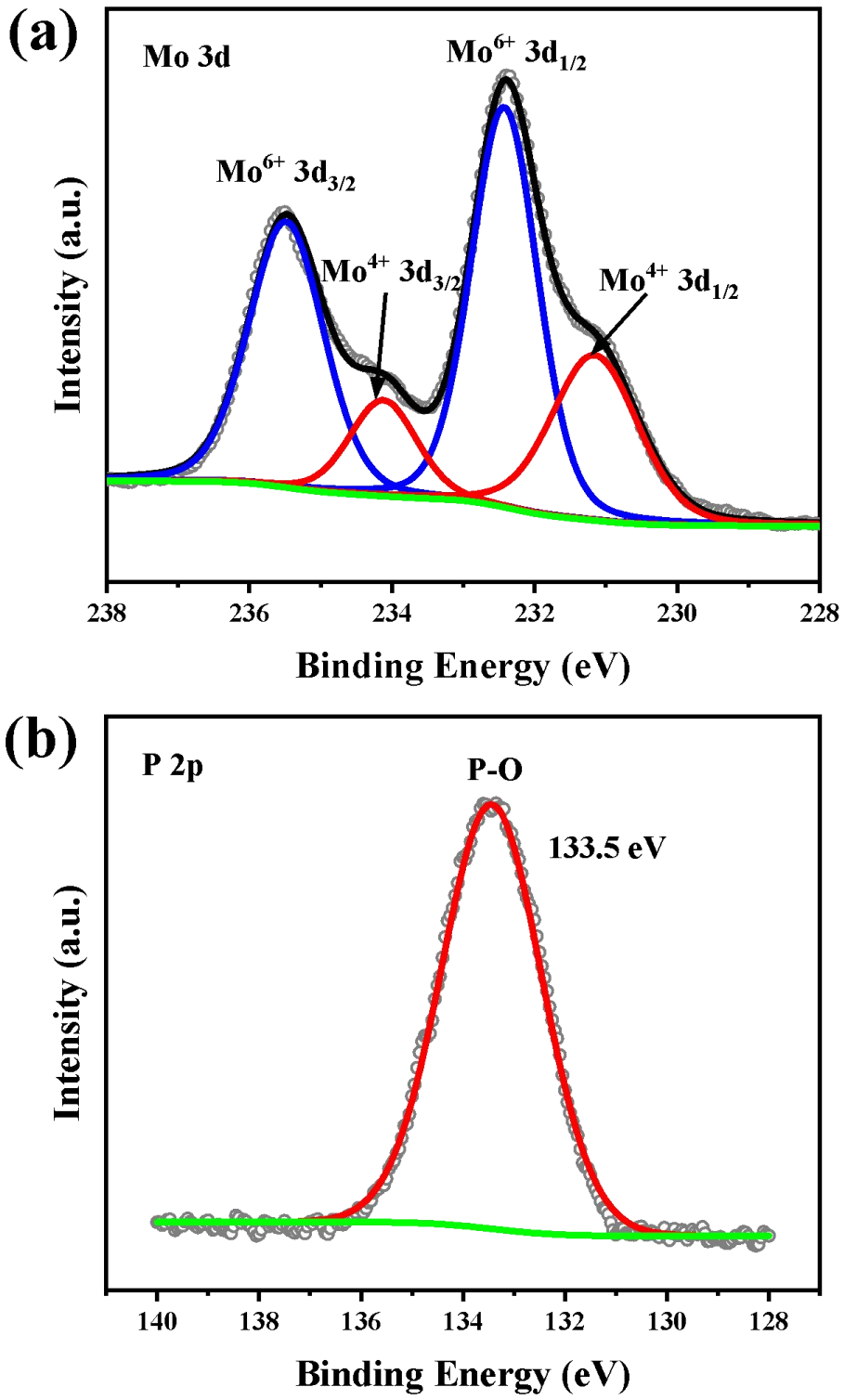

Supplementary Figure 12. High-resolution spectra of (a) Mo 3d and (b) P 2p for P-FeNiMoO.

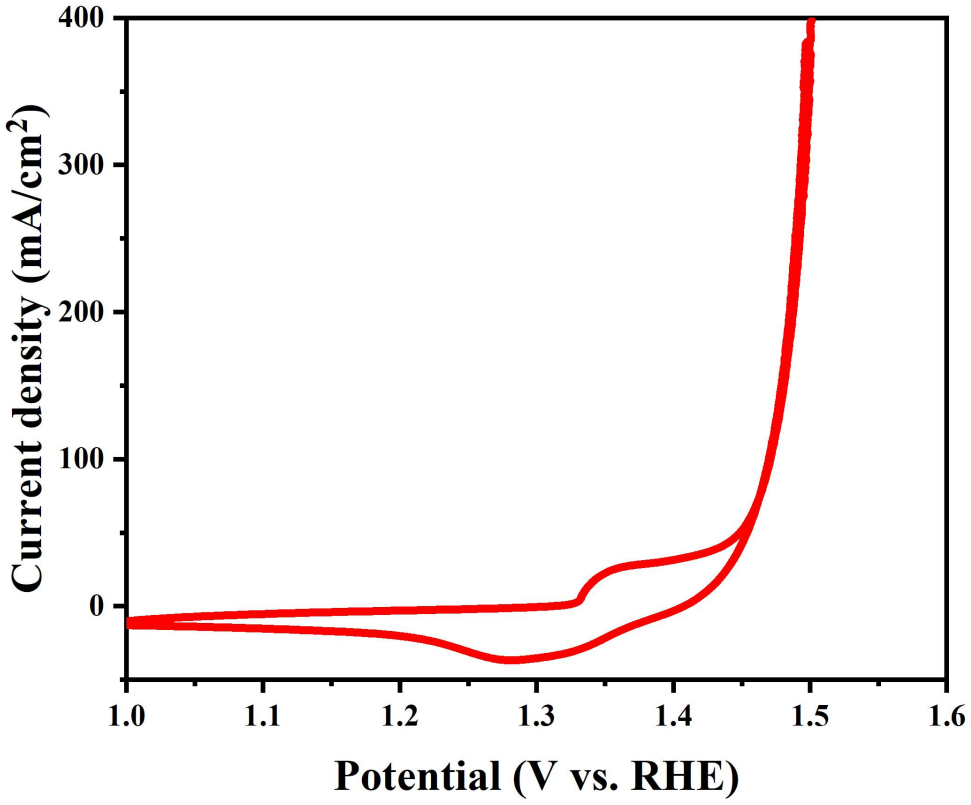

Supplementary Figure 13. CV polarization curve of P-NiFe@$NiMoO_4$.

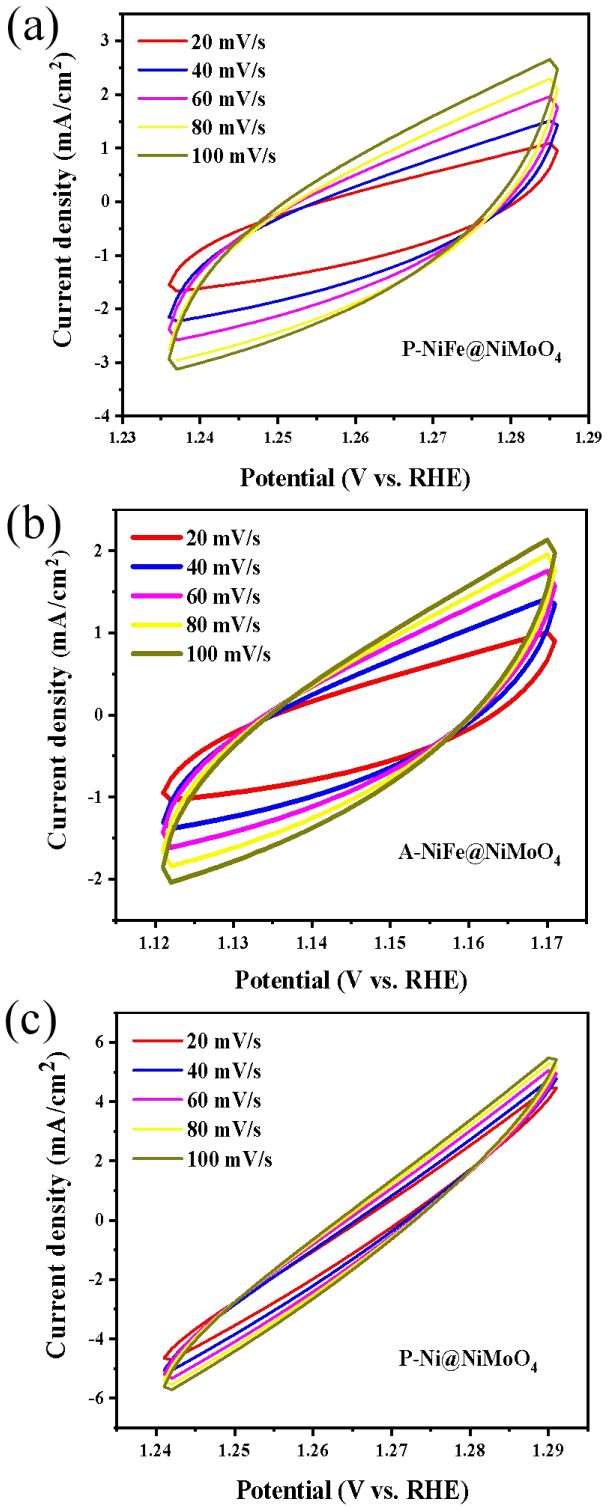

Supplementary Figure 14. CV curves of (a) P-NiFe@$NiMoO_4$, (b) A-NiFe@$NiMoO_4$, and (c) P-Ni@$NiMoO_4$ at scan rates ranging from 20 mV s^{-1} to 100 mV s^{-1} with an interval point of 20 mV s^{-1}.

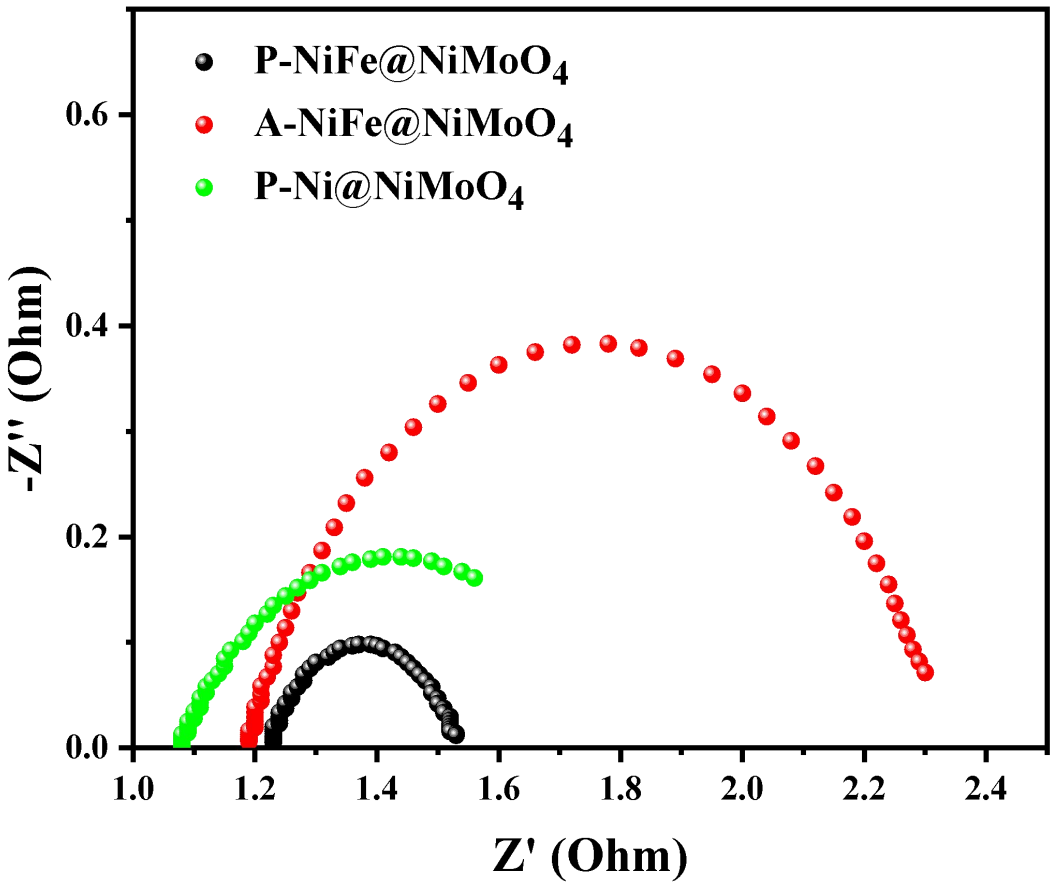

Supplementary Figure 15. EIS Nyquist plots of different catalysts tested at a potential of 1.6 V vs. RHE.

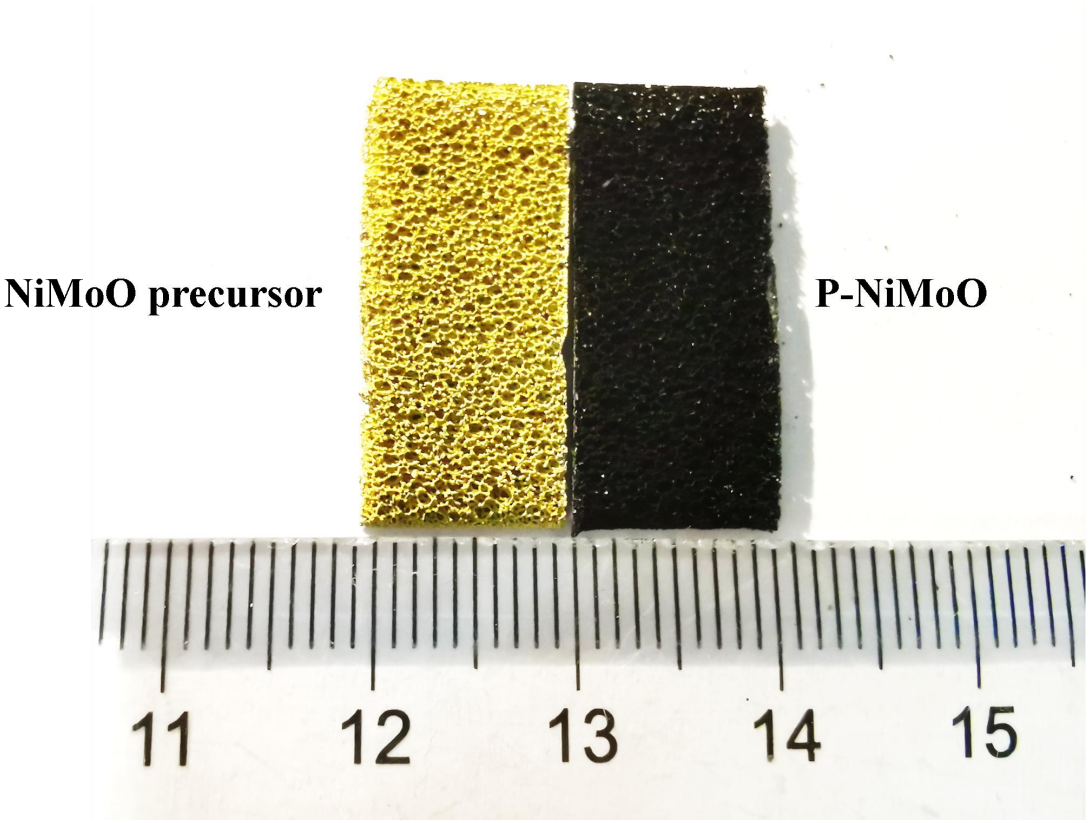

Supplementary Figure 16. Optical image of NiMoO precursor (L) and P-NiMoO (R).

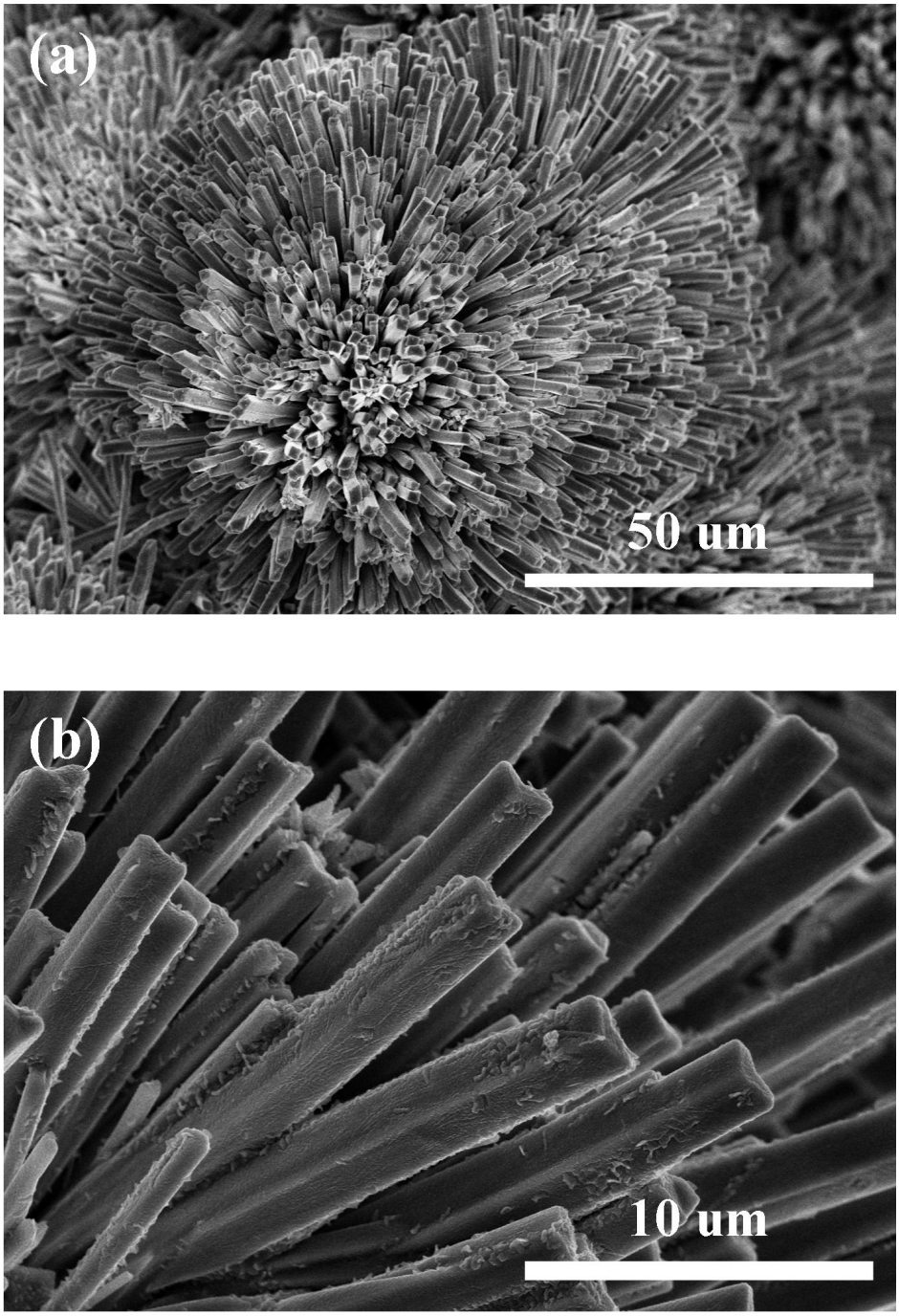

Supplementary Figure 17. SEM images of P-NiMoO at different magnification.

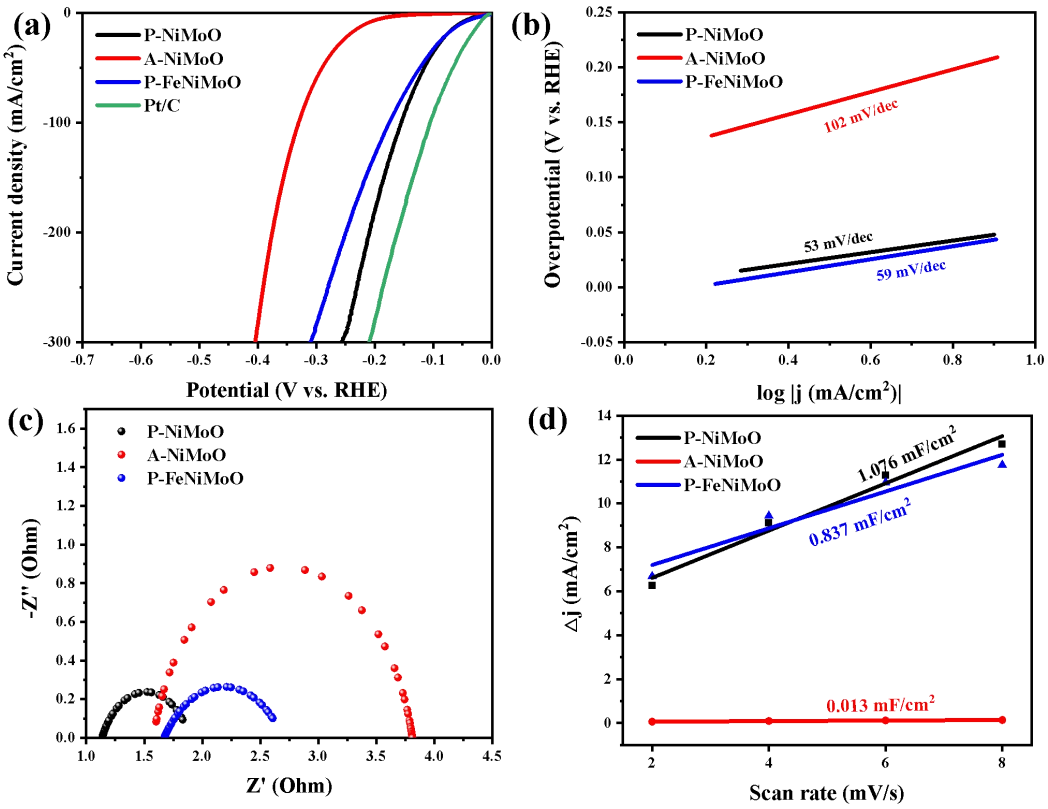

Supplementary Figure 18. (a) Polarization curves of P-NiMoO, A-NiMoO, P-FeNiMoO, and commercial Pt/C for HER in 1M KOH. The corresponding (b) Tafel plots, (c) EIS Nyquist plots, and (d) C_{dl} values of the above electrodes.

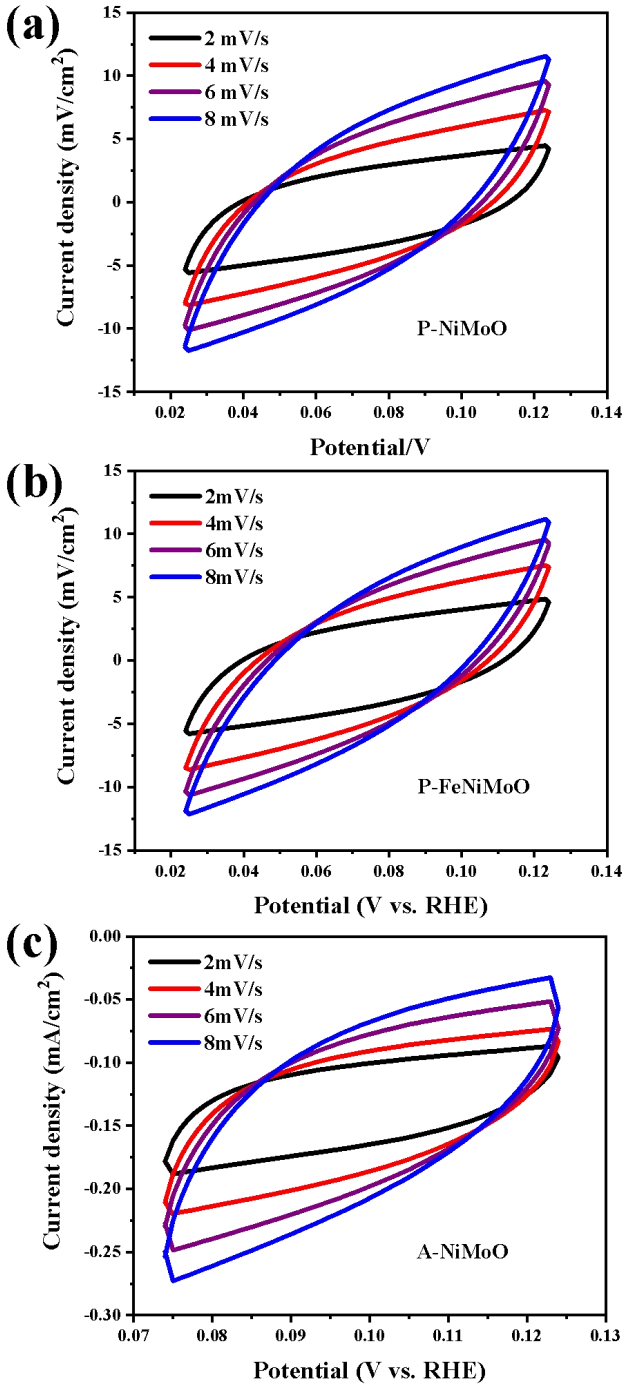

Supplementary Figure 19. CV curves of (a) P-NiMoO, (b) P-FeNiMoO, and (c) A-NiMoO electrode at scan rates ranging from 2 to 8 mV s^{-1} with an interval of 2 mV s^{-1}.

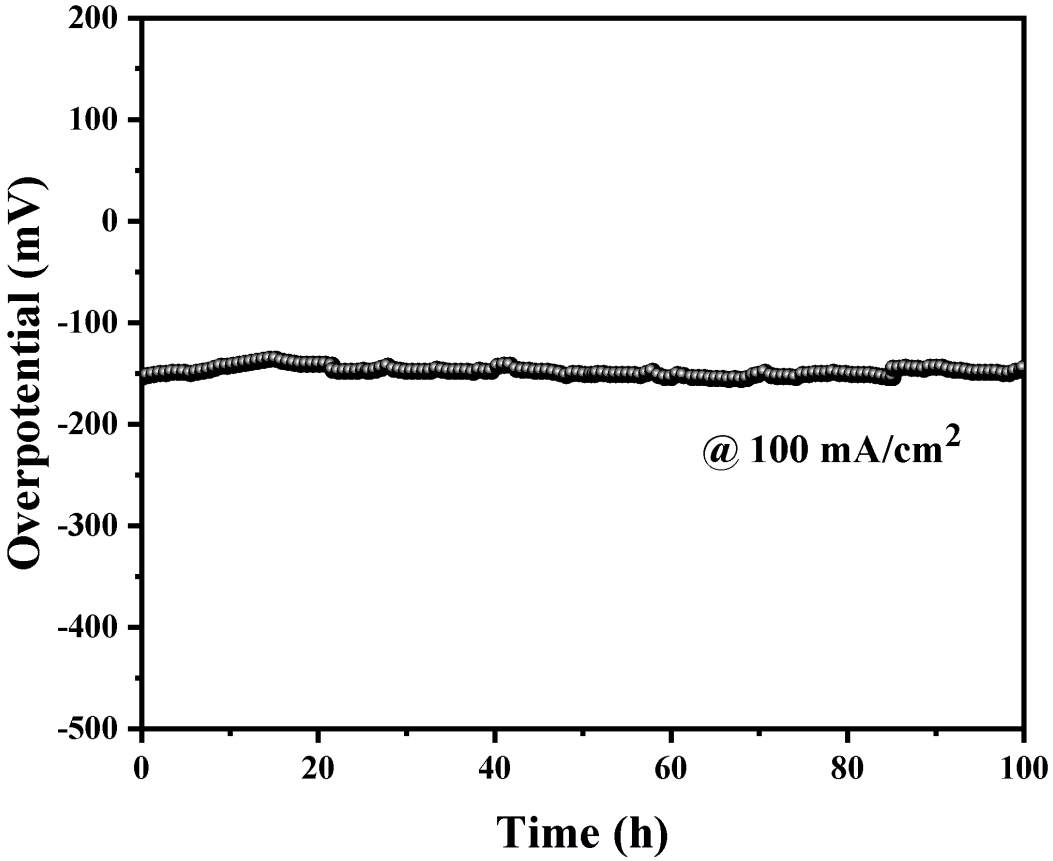

Supplementary Figure 20. Chronopotentiometry curve of P-NiMoO electrode at a current density of 100 mA cm^{-2} in 1M KOH.

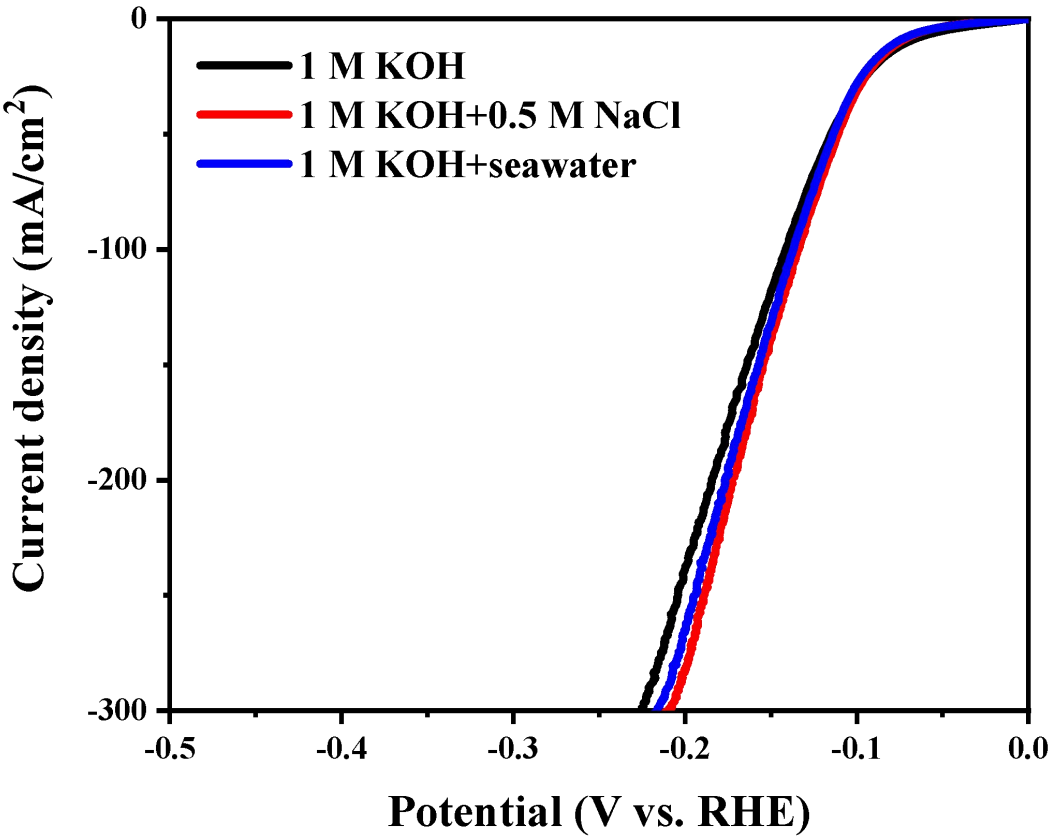

Supplementary Figure 21. Polarization curves of P-NiMoO electrode tested in different electrolytes in 1M KOH at 25 ℃.

Supplementary Figure 22. The gas collecting device of evolved H_2 and O_2.

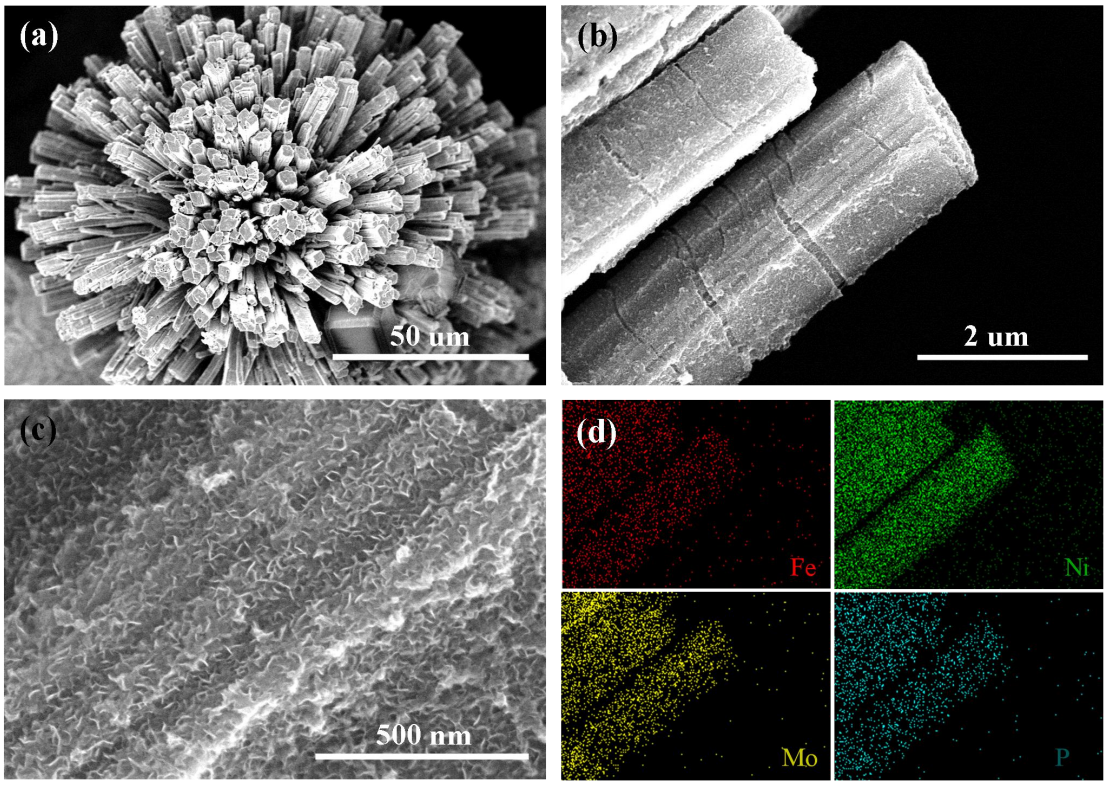

Supplementary Figure 23. (a-c) SEM and (d) elemental mapping images of P-NiFe@$NiMoO_4$ after 200h seawater electrolysis at 100 mA/cm^2 in 1M KOH+ seawater at 25 ℃.

Supplementary Table 1. The element content of P-FeNiMoO and P-NiFe@$NiMoO_4$ from the XPS survey.

Sample	Content (at%)					
	Ni	**Fe**	**Mo**	**P**	**O**	**C**
P-FeNiMoO	9.89	3.89	7.23	7.47	52.48	19.04
P-NiFe@$NiMoO_4$	14.62	5.31	0.36	7.58	51.8	20.33

Supplementary Table 2. Comparison of OER performance for the samples of this work and other reported catalysts. (η_{100} -overpotential at 100 mA/cm^2)

Catalyst	Electrolyte	η_{100} (mV)	Reference
P-NiFe@$NiMoO_4$	**1 M KOH**	**238**	**This work**
$Zn_{0.2}Co_{0.8}OOH$	1 M KOH	290*	1
Se-doped FeOOH	1 M KOH	279	2
NiCoFe-MOF	1 M KOH	310*	3
FeNiP/NCH	1 M KOH	340*	4
$Fe_xCo_{1-x}OOH$	1 M KOH	300*	5
NiFeRu LDH	1 M KOH	260	6
NiFeV	1 M KOH	264	7
Co-Ni_3N	1 M KOH	385*	8
Cu@NiFe LDH	1 M KOH	281	9
NiFe LDH/graphene	1 M KOH	325*	10
NiFe-OH/NiFeP	1 M KOH	245	11
FeCoW	1 M KOH	253*	12
NiFe LDH	1 M KOH	450*	13

* The value was calculated from the curve shown in the reference.

Supplementary Table 3. Comparison of water splitting performance of Fe-$NiMoO_4$-P-EO/NF|| $NiMoO_4$-P/NF cell in this work with other reported catalysts. (V_{100} -cell voltage at 100 mA/cm^2)

Catalyst	Electrolyte	V_{100} (V)	Reference
P-NiFe@$NiMoO_4$|| P-NiMoO	**1 M KOH** **1 M KOH+seawater**	**1.63** **1.63**	**This work**
NiVIr-LDH||NiVRu-LDH	1 M KOH	1.67*	14
Ni_2P-Fe_2P/NF|| Ni_2P-Fe_2P/NF	1 M KOH 1 M KOH+seawater	1.7 1.79	15
S-(Ni,Fe)OOH||NiMoN	1 M KOH+1 M NaCl 1 M KOH+seawater	1.631 1.661	16
S:CoP@NF||S:CoP@NF	1 M KOH	1.78	17
$NiFeO_x$||NiFe-P	1 M KOH	1.76*	18
$MoNi_4/MoS_2$||Ni_3S_2	1 M KOH	1.67	19

* The value was calculated from the curve shown in the reference.

References

1. Huang Z, Song J, Du Y et al. Chemical and structural origin of lattice oxygen oxidation in Co–Zn oxyhydroxide oxygen evolution electrocatalysts. *Nat Energy* 2019;4:329-338. [DOI: 10.1038/s41560-019-0355-9]
2. Niu S, Jiang W, Wei Z et al. Se-Doping Activates FeOOH for Cost-Effective and Efficient Electrochemical Water Oxidation. *J Am Chem So*. 2019;141:7005-7013. [DOI: 10.1021/jacs.9b01214]
3. Qian Q, Li Y, Liu Y, Yu L, Zhang G. Ambient Fast Synthesis and Active Sites Deciphering of Hierarchical Foam-Like Trimetal-Organic Framework Nanostructures as a Platform for Highly Efficient Oxygen Evolution Electrocatalysis. *Adv Mater* 2019;31:e1901139. [DOI: 10.1002/adma.201901139]
4. Wei Y, Zhang M, Kitta M, Liu Z, Horike S, Xu Q. A Single-Crystal Open-Capsule Metal-Organic Framework. *J Am Chem Soc* 2019;141:7906-7916. [DOI: 10.1021/jacs.9b02417]
5. Ye S, Shi Z, Feng J, Tong Y, Li G. Activating CoOOH Porous Nanosheet Arrays by Partial Iron Substitution for Efficient Oxygen Evolution Reaction. *Angew Chem Int Ed Engl* 2018;57:2672-2676. [DOI: 10.1002/anie.201712549]
6. Chen G, Wang T, Zhang J et al. Accelerated Hydrogen Evolution Kinetics on NiFe-Layered Double Hydroxide Electrocatalysts by Tailoring Water Dissociation Active Sites. *Adv Mater* 2018;30:1706279. [DOI: 10.1002/adma.201706279]
7. Jiang J, Sun F, Zhou S et al. Atomic-level insight into super-efficient electrocatalytic oxygen evolution on iron and vanadium co-doped nickel (oxy)hydroxide. *Nat Commun.* 2018;9:85. [DOI: 10.1038/s41467-018-05341-y]
8. Zhu C, Wang A, Xiao W. In Situ Grown Epitaxial Heterojunction Exhibits High-Performance Electrocatalytic Water Splitting. *Adv Mater* 2018;30:e1705516. [DOI: 10.1002/adma.201705516]
9. Yu L, Zhou H, Sun J et al. Cu nanowires shelled with NiFe layered double hydroxide nanosheets as bifunctional electrocatalysts for overall water splitting.

Energy Environ Sci 2017;10:1820-1827. [DOI: 10.1039/C7EE01571B]

10. Jia Y, Zhang L,Gao, G. A Heterostructure Coupling of Exfoliated Ni-Fe Hydroxide Nanosheet and Defective Graphene as a Bifunctional Electrocatalyst for Overall Water Splitting. *Adv Mater* 2017;29:1700017. [DOI: 10.1002/adma.201700017]
11. Liang H, Gandi A, Xia C et al. Amorphous NiFe-OH/NiFeP Electrocatalyst Fabricated at Low Temperature for Water Oxidation Applications. *ACS Energy Lett* 2017;2:1035-1042. [DOI: 10.1021/acsenergylett.7b00206]
12. Zhang B, Zheng X, Voznyy O et al. Homogeneously dispersed multimetal oxygen-evolving catalysts. *Science* 2016;352:333-337. [DOI: 10.1126/science.aaf1525]
13. Luo J, Im J, Mayer, M et al. Water photolysis at 12.3% efficiency via perovskite photovoltaics and Earth-abundant catalysts. *Science* 2014;345:1593-1596. [DOI: 10.1126/science.1258307]
14. Wang D, Li Q, Han C, Lu Q, Xing Z, Yang X. Atomic and electronic modulation of self-supported nickel-vanadium layered double hydroxide to accelerate water splitting kinetics. *Nat Commun* 2019;10:3899. [DOI: 10.1038/s41467-019-11765-x]
15. Wu L, Yu L, Zhang F et al. Heterogeneous Bimetallic Phosphide Ni_2P-Fe_2P as an Efficient Bifunctional Catalyst for Water/Seawater Splitting. *Adv Funct Mater* 2020;31:2006484. [DOI: 10.1002/adfm.202006484]
16. Yu L, Wu L, McElhenny B et al. Ultrafast room-temperature synthesis of porous S-doped Ni/Fe (oxy)hydroxide electrodes for oxygen evolution catalysis in seawater splitting. *Energy Environ Sci* 2020l13:3439-3446. [DOI: 10.1039/D0EE00921K]
17. Anjum M, Okyay M, Kim M, Lee M, Park N, Lee J. Bifunctional sulfur-doped cobalt phosphide electrocatalyst outperforms all-noble-metal electrocatalysts in alkaline electrolyzer for overall water splitting. *Nano Energy* 2018;53:286-295. [DOI: 10.1016/j.nanoen.2018.08.064]

18. Wang J, Ji L, Zuo S, Chen Z. Hierarchically Structured 3D Integrated Electrodes by Galvanic Replacement Reaction for Highly Efficient Water Splitting. *Adv Energy Mater* 2017;7:1700107. [DOI: 10.1002/aenm.201700107]
19. Zhang J, Wang T, Liu P et al. Efficient hydrogen production on $MoNi_4$ electrocatalysts with fast water dissociation kinetics. *Nat Commun* 2017;8:15437. [DOI: 10.1038/ncomms15437]